Substrate-Assisted Cysteine Deprotonation in the Mechanism of Dimethylargininase (DDAH) from *Pseudomonas aeruginosa*†

Everett M. Stone,‡ Alison L. Costello,§ David L. Tierney,*,§ and Walter Fast*,‡,||

Division of Medicinal Chemistry, College of Pharmacy, Graduate Programs in Biochemistry and Cell and Molecular Biology, The University of Texas at Austin, Austin, Texas 78712, and Department of Chemistry, University of New Mexico, Albuquerque, New Mexico 87131

Received December 20, 2005; Revised Manuscript Received March 13, 2006

ABSTRACT: The enzyme dimethylargininase (also known as dimethylarginine dimethylaminohydrolase or DDAH; EC 3.5.3.18) catalyzes the hydrolysis of endogenous nitric oxide synthase inhibitors, N^{ω}-methyl-L-arginine and N^{ω},N^{ω}-dimethyl-L-arginine. Understanding the mechanism and regulation of DDAH activity is important for developing ways to control nitric oxide production during angiogenesis and in many cases of vascular endothelial pathobiology. Several possible physiological regulation mechanisms of DDAH depend upon the presence of an active-site cysteine residue, Cys249 in *Pseudomonas aeruginosa* (*Pa*) DDAH, which is proposed to serve as a nucleophile in the catalytic mechanism. Through the use of pH-dependent ultraviolet and visible (UV−vis) difference spectroscopy and inactivation kinetics, the pK_a of the active-site Cys249 in the resting enzyme was found to be unperturbed from pK_a values of typical noncatalytic cysteine residues. In contrast, the pH dependence of k_{cat} values indicates a much lower apparent pK_a value. UV−vis difference spectroscopy between wild-type and C249S DDAH shows absorbance changes consistent with Cys249 deprotonation to the anionic thiolate upon binding positively charged ligands. The proton from Cys249 is lost either to the solvent or to an unidentified general base. A mutation of the active-site histidine residue, H162G, does not eliminate cysteine nucleophilicity, further arguing against a pre-formed ion pair with Cys249. Finally, UV−vis and X-ray absorption spectroscopy revealed that inhibitory metal ions can bind at these two active-site residues, Cys249 and His162, and also stabilize the anionic form of Cys249. These results support a proposed substrate-assisted mechanism for *Pa* DDAH in which ligand binding modulates the reactivity of the active-site cysteine.

In humans, the plasma concentration of asymmetric N^{ω},N^{ω}-dimethyl-L-arginine (ADMA)[1] is a biochemical marker associated with serious cardiovascular risk factors including hypercholesterolemia, hyperhomocysteinemia, diabetes, and hypertension (*1*). This alkylated arginine residue and the related compound N^{ω}-methyl-L-arginine are endogenous inhibitors of nitric oxide (·NO) synthase (*2*, *3*). A growing body of evidence indicates that these arginine derivatives can regulate ·NO production in vivo and that increases in plasma ADMA levels may actually mediate the vascular endothelial pathobiology common to many of these disorders (*1*). The enzyme dimethylargininase (also known as dimethylarginine dimethylaminohydrolase or DDAH; EC 3.5.3.18) catalyzes the guanidino hydrolysis of these N^{ω}-alkylated arginine residues to yield citrulline and alkylamine products (Scheme 1) and may serve as a control point for regulating the concentration of ADMA and, in turn, ·NO production (*1*). The ability of DDAH isoforms to control levels of ADMA and ·NO production has also been linked to angiogenesis (*4*). For example, the overexpression of rat DDAH-1 in a C6 rat glioma cell line was found to increase ·NO synthesis, increase expression and secretion of vascular endothelial cell growth factor (VEGF, a growth factor known to stimulate angiogenesis), induce angiogenesis [particularly the early stages of vasculogenesis (*5*)], and lead to tumors that grow twice as fast as the wild type (*6*). Therefore, new

† This research was supported by the Robert A. Welch Foundation (F-1572 to W.F.), the American Cancer Society (RSG-05-061-01-GMC to W.F.), and the National Institutes of Health (P20RR-16480 from the BRIN/INBRE Program of the National Center for Research Resources to D.L.T.). The National Synchrotron Light Source is supported by the U.S. Department of Energy.

* To whom correspondence should be addressed: The University of Texas at Austin, College of Pharmacy, PHAR-MED CHEM, 1 University Station, A1935, Austin, TX 78712. Telephone: (512) 232-4000. Fax: (512) 232-2606. E-mail: waltfast@mail.utexas.edu (W.F.); The University of New Mexico, Department of Chemistry, Albuquerque, NM 87131. Telephone: (505) 277-2505. Fax: (505) 277-2609. E-mail: dtierney@unm.edu (D.L.T.).

‡ Graduate Program in Cell and Molecular Biology, The University of Texas at Austin.

§ University of New Mexico.

|| Division of Medicinal Chemistry and Graduate Program in Biochemistry, The University of Texas at Austin.

[1] Abbreviations: ·NO, nitric oxide; DDAH, dimethylarginine dimethylaminohydrolase; ADMA, asymmetric N^{ω},N^{ω}-dimethyl-L-arginine; *Pa*, *Pseudomonas aeruginosa*; His_6, hexahistidine affinity tag; ESI−MS, electrospray ionization−mass spectrometry; UV−vis, ultraviolet and visible; calcd, calculated; equiv, equivalent; LMCT, ligand-to-metal charge transfer; VEGF, vascular endothelial cell growth factor; EDTA, ethylenediaminetetraacetic acid; MES, 2-morpholinoethanesulfonic acid; HEPES, 4-(2-hydroxyethyl)-1-piperazineethane sulfonic acid; NSLS, National Synchrotron Light Source; IC_{50}, the concentration of the inhibitor required to produce 50% inhibition of the enzyme activity in the presence of a defined amount of substrate; Abs, absorbance; EXAFS, extended X-ray absorption fine spectroscopy.

10.1021/bi052595m CCC: $33.50
Published on Web 04/07/2006

Scheme 1: Proposed Mechanism for DDAH-Catalyzed Hydrolysis of Asymmetric N^{ω},N^{ω}-Dimethyl-L-arginine

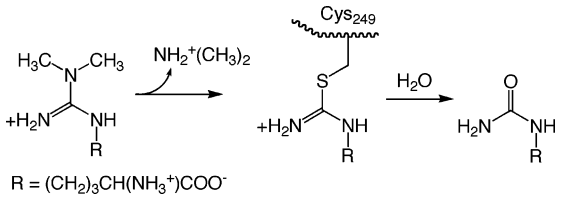

inhibitors that control DDAH activity are of significant interest (*7*).

Several physiological mechanisms for regulating DDAH activity have been proposed, including inhibition by S-nitrosylation as feedback inhibition during •NO overproduction (*8*, *9*), covalent bond formation with L-homocysteine (*10*) and *S*-nitroso-L-homocysteine (*11*) during oxidative and nitrosative stress, and metal binding (*9*, *12*−*14*). All of these mechanisms involve key interactions with the active-site cysteine residue of DDAH, although there appears to be some differences between isoforms (*8*, *9*). Understanding the reactivity of the active-site cysteine and its role in catalysis and regulation are clearly important for determining how these enzymes control ADMA levels, thereby setting the stage for future drug design.

The active-site cysteine (Cys249) is essential in the proposed mechanism of DDAH (Scheme 1), which proceeds through the attack of this cysteine residue on the guanidinium carbon of the substrate. The collapse of the resulting tetrahedral adduct expels the alkylamine leaving group and generates a covalent thiouronium intermediate with sp^2 hybridization (Scheme 1). Subsequent hydrolysis of this intermediate yields the product citrulline. This mechanism is thought to be similar to other enzymes in the amidinotransferase superfamily in which covalent intermediates are involved (*15*−*18*). Mutagenesis (*19*), crystallography (*19*), and intermediate-trapping experiments (*20*) support the role of the active-site cysteine (Cys249) in *Pseudomonas aeruginosa* (*Pa*) DDAH as the catalytic nucleophile, but the mechanisms of cysteine deprotonation and intermediate hydrolysis are not as clear. In general, DDAH isoforms are active at neutral and acidic pH values, yet there are no protein residues obviously positioned to lower the pK_a of the active-site cysteine to enhance its nucleophilicity. Also, at least two different mechanisms for hydrolysis of the covalent intermediate have been proposed for enzymes in this superfamily (*21*, *22*). Finally, zinc binds very tightly to the active-site cysteine of bovine DDAH-1, which may regulate enzyme activity and protect against S-nitrosylation (*9*, *13*). However, the S-nitrosylation patterns in bovine and *Pa* DDAH isoforms appear to be different; bovine DDAH-1 is easily nitrosylated on two cysteine residues (*9*), but *Pa* DDAH is only readily nitrosylated at the active-site cysteine (*8*). These observations suggest that, despite similar sequences, there may be significant functional differences between DDAH active sites.

In this work, we report results indicating that the active-site cysteine is protonated in the resting enzyme but is deprotonated when cationic ligands, such as substrate, lysine, or metal ions, are bound. The proton from Cys249 is lost either to the solvent or to an unidentified general base. We also report results indicating that the active-site histidine residue is essential for deprotonating the water used to hydrolyze the covalent thiouronium intermediate. These findings are consistent with a substrate-assisted mechanism for *Pa* DDAH, which can be competitively inhibited by metal binding at the active site. These mechanistic details illustrate how *Pa* DDAH uses ligand binding to alter the nucleophilicity of the active-site cysteine and may help to illuminate differences in physiological regulation between DDAH isoforms.

MATERIALS AND METHODS

Materials. Unless noted otherwise, all chemicals are from Sigma−Aldrich Chemical Co. (St. Louis, MO). All enzymes, including wild-type *Pa* DDAH and the catalytically inactive C249S and H162G *Pa* DDAH mutants, were purified and assayed as described previously (*20*, *23*−*25*).

pH Dependence of Pa DDAH-Catalyzed Hydrolysis of S-Methyl-L-thiocitrulline. Because thiol reactivity changes with pH, the continuous assay for DDAH based on 5,5′-dithiobis-(2-nitrobenzoic acid) (*24*) was not used for these experiments. Instead, a new assay based on the inherent spectral differences between *S*-methyl-L-thiocitrulline and the products, methanethiol and L-citrulline, was used to directly monitor substrate hydrolysis in a continuous manner by following absorbance decreases in the UV spectrum. Multiple wavelengths were monitored to quantify different concentration ranges, typically using 260 nm for high substrate concentrations (0.6−8 mM), 245 nm for lower concentrations (0.125−0.6 mM), and 235 nm for the lowest concentrations (0.015−0.125 mM). Standard curves were prepared either using *S*-methyl-L-thiocitrulline or using equimolar mixtures of L-citrulline and methanethiol to quantify the observed absorbance changes. Including methanethiol in these standard curves is particularly important at alkaline pH values because thiolates have a higher absorbance than protonated thiols. The accuracy of this method was verified through a comparison with parallel reactions at one selected pH (7.3), which were assayed using both a discontinuous assay for citrulline production (*23*) and a continuous spectrophotometric assay (*24*). Typically, reactions of *Pa* DDAH (1−3.5 μM) with *S*-methyl-L-thiocitrulline (concentrations from 0 to 10× K_M) were prepared at various pH values (4.5−9.5) using the following buffers: at pH 4.5−5, sodium acetate (250 mM); at pH 5.5−6.5, 2-morpholinoethanesulfonic acid (MES) (250 mM); at pH 7−7.5, 4-(2-hydroxyethyl)-1-piperazineethane sulfonic acid (HEPES) (250 mM); at pH 8−8.5, Tris-HCl (250 mM); and at pH 9−9.5, sodium borate (250 mM). All buffers contain KCl (250 mM). All reactions were done at least in triplicate at each pH value, and the observed rates were fit to the Michaelis−Menten equation using the software Kaleidagraph (Synergy) to obtain the steady-state rate constants.

pH Dependence of Pa DDAH-Catalyzed Hydrolysis of N^{ω}-Methyl-L-arginine. A previously published discontinuous assay for L-ctirulline production (*23*) was used to determine the steady-state rate constants for *Pa* DDAH-catalyzed hydrolysis of N^{ω}-methyl-L-arginine using the same conditions as described for *S*-methyl-L-thiocitrulline. All reactions were performed at least in triplicate, and the observed results were fit directly to the Michaelis−Menten equation.

Fitting the Steady-State pH-Rate Data. Fits to the resulting k_{cat}/K_M values and k_{cat} values for hydrolysis of both substrates

at each pH were calculated as described below. Bell-shaped curves were fit with a two pK_a model (eq 1), rearranged as shown in eq 2, in which y is substituted by either k_{cat}/K_M or k_{cat}, accordingly (*26*), and a lower limiting term, y_{min}, was added to allow for a nonzero plateau at low pH values. This y_{min} term was fixed at 0 when fitting data from N^{ω}-methyl-L-arginine hydrolysis but was left unconstrained to obtain good fits to data from *S*-methyl-L-thiocitrulline hydrolysis. Because fits to two pK_a values closer than 3.5 units tend to underestimate y_{max}, Segel's method (eqs 3 and 4) was used to calculate corrected pK_a values for each limb of the k_{cat}/K_M profiles (*26*).

$$\log[y_{obs}] = \log[y_{max}] - \log\left[1 + \frac{[H^+]}{K_1} + \frac{K_2}{[H^+]}\right] \quad (1)$$

$$\log[y_{obs}] = \log\left[y_{min} + \frac{(y_{max} - y_{min})}{(1 + 10^{(pK_{a1} - pH)} + 10^{(pH - pK_{a2})})}\right] \quad (2)$$

$${}_1[H^+]_{1/2} + {}_2[H^+]_{1/2} = K_1 + 4[H^+]_{opt} \quad (3)$$

$$[H^+]_{opt} = \sqrt{K_1 K_2} \quad (4)$$

Fits to the k_{cat} values for *S*-methyl-L-thiocitrulline hydrolysis at each pH were calculated using a single pK_a model including a lower limiting term, k_{min}, to account for the nonzero plateau at low pH as described in eq 5.

$$\log[k_{cat}] = \log\left[k_{min} + \frac{(k_{max} - k_{min})}{(1 + 10^{(pK_a - pH)})}\right] \quad (5)$$

Ultraviolet and Visible (UV−Vis) Difference Spectroscopy of Apoproteins. Stock solutions of hexahistidine affinity tag (His_6)-tagged *Pa* DDAH (70 μM) and His_6-tagged *Pa* C249S DDAH (120 μM) were prepared as described earlier (*20*) and then diluted to final concentrations of 8.3 and 14.1 μM, respectively, using various buffers with pH values between 6 and 10. The following buffers were used at the pH ranges as indicated: at pH 5.5−6.5, MES (20 mM); at pH 7−8, HEPES (20 mM); and at pH 8.5−10, 2-(cyclohexylamino)-ethylsulfonic acid (CHES) (20 mM). All buffers contain KCl (100 mM). The absorbance of each sample at 240 and 280 nm was measured in at least three separate experiments using a quartz microcuvette and a Cary 50 UV−vis spectrophotometer (Varian, Inc., Walnut Creek, CA), after the baseline correction using the appropriate buffer as a blank. The resulting absorbance values at 240 nm were normalized using the 280 nm readings and then averaged for each pH value. The (Abs_{240}/Abs_{280}) ratio for the C249S mutant was then subtracted from the (Abs_{240}/Abs_{280}) ratio determined for wild-type *Pa* DDAH at each pH and then multiplied by the calculated native extinction coefficient for *Pa* DDAH (ϵ_{280} = 20 240 M^{-1} cm^{-1}) to determine the observed $\Delta\epsilon_{240}$ values at each pH. The Grubbs test, calculated with an α value of 0.05 using the GraphPad outlier calculator available free of charge from http://www.graphpad.com/quickcalcs/Grubbs1.cfm, was used to remove any outlying data points. To determine the observed pK_a for the absorbance changes at 240 nm, the program KaleidaGraph (Synergy Software, Reading, PA) was used to fit eq 6, in a procedure similar to that reported previously (*27*).

$$\epsilon_{240(obs)} = \epsilon_{240(min)} + \frac{(\epsilon_{240(max)} - \epsilon_{240(min)})}{(1 + 10^{(pK_a - pH)})} \quad (6)$$

pH Dependence of Pa DDAH Inactivation by Iodoacetamide. Preincubation mixtures of *Pa* DDAH (11 μM) with varying concentrations of iodoacetamide (0−2.5 mM) were prepared at various pH values (5.5−10) in the buffers described above. At pH values from 5.5 to 7.5, aliquots of the preincubation mixtures were withdrawn at successive time points, diluted 26-fold into an assay buffer containing an excess of the alternative substrate *S*-methyl-L-thiocitrulline (1 mM), potassium phosphate (100 mM), ethylenediaminetetraacetic acid (EDTA) (1 mM), and 5,5′-dithiobis-(2-nitrobenzoic acid) (200 μM) at pH 7.3, and the remaining enzyme activity was monitored using a continuous spectrophotometric assay as described previously (*25*). Under these conditions, the diluted iodoacetamide does not significantly interfere with the activity assay. At pH values greater than 8, only single time points were assayed because of the increased rate of inactivation. A form of the second-order rate equation (eq 7) was used to obtain rate constants for inactivation in a procedure similar to that described elsewhere (*28*). Act_{obs} and Act_{inital} are the observed and initial percent enzyme activities, [I] is the initial iodoacetamide concentration, and t is the preincubation time.

$$A_{obs} = A_{initial} e^{-k[I]t} \quad (7)$$

To determine the observed pK_a for inactivation by iodoacetamide, the resulting $k_{inact(obs)}$ values, determined at each pH, were fitted with a single apparent pK_a value (eq 8). All experiments and controls were performed at least in triplicate.

$$k_{inact(obs)} = \frac{(k_{inact(max)})}{(1 + 10^{(pK_a - pH)})} \quad (8)$$

Mass Spectrometry of Quenched Reactions. Typically, steady-state reactions with *Pa* DDAH (final concentration of 50 μM) and substrate (5 mM) were incubated for 20−30 s at 25 °C before the addition of trifluoroacetic acid (final concentration of 1 M), which quenches the reactions during turnover and traps any acid-stable covalent intermediates that accumulate. Incubations at two different pH values were prepared in the following buffers: at pH 5.5, MES (200 mM) and at pH 8, Tris-HCl (200 mM). Both buffers contain KCl (200 mM). Quenched reactions were analyzed by electrospray ionization−mass spectrometry (ESI−MS) as described previously (*20*). Incubations with the H162G mutant (25−50 μM) were also completed using slightly more substrate (5−10 mM), longer reaction times (3−10 min), and even repeated at a higher pH (9.5) to maximize the chance of trapping potential intermediates during incubations with N^{ω},N^{ω}-dimethyl-L-arginine.

Inhibition of Pa DDAH by L-Lysine. The steady-state rates of *Pa* DDAH (670 nM) catalyzed hydrolysis of *S*-methyl-L-thiocitrulline (8−1000 μM) were determined in varying concentrations of L-lysine (1.25−15 mM) in K_2HPO_4 (0.1 M) buffer and EDTA (1 mM) at 25 °C and pH 7.3 using a continuous assay as described earlier (*24*). All reactions were

done in triplicate, and the results were directly fit using KaleidaGraph software (Synergy) to eq 9 for competitive inhibition (*29*), where $\alpha = (1 + [I]/K_i)$

$$v = \frac{k_{cat}[S][E]_{total}}{(\alpha K_M + [S])} \quad (9)$$

UV−Vis Difference Spectroscopy of Ligand-Bound Proteins. Using a quartz microcuvette and a Cary 50 UV−vis spectrophotometer (Varian, Inc.), absorbance scans (230−300 nm) were recorded for wild-type and C249S mutant *Pa* DDAH (4−5 μM) in K_2HPO_4 buffer (100 mM) and EDTA (1 mM) at pH 7.3 in the presence of either L-lysine (10 mM) or L-citrulline (20 mM) at concentrations required to achieve approximately 70% saturation. Baseline corrections were made using control solutions in which the protein component was omitted. All experiments were repeated at least in triplicate, and an average observed extinction coefficient was calculated at each wavelength as described above. The ligand-dependent changes in the observed extinction coefficient at each wavelength were then calculated for both wild-type and C249S mutant *Pa* DDAH by subtracting the results from the L-citrulline-bound proteins from those of the L-lysine-bound proteins at each wavelength.

Inhibition of Pa DDAH by Zinc(II). The concentration of zinc(II) required to inhibit 50% of *Pa* DDAH activity (IC_{50}) was determined by assaying the hydrolysis rates for *S*-methyl-L-thiocitrulline (50 μM) in the presence of *Pa* DDAH (840 nM), Tris-HCl buffer (250 mM), and KCl (250 mM) at 25° and pH 7.5 with increasing concentrations of zinc acetate (0−10 μM) using a continuous assay as described previously (*24*). Using the determined IC_{50} value, a K_i value for zinc(II) inhibition of *Pa* DDAH was estimated using eq 10 (*30*), assuming competitive inhibition, and using a K_M for *S*-methyl-L-thiocitrulline (46 ± 4 μM) determined under identical conditions.

$$K_i = \frac{IC_{50}}{\left(1 + \frac{[S]}{K_M}\right)} \quad (10)$$

Extended X-ray Absorption Fine Spectroscopy (EXAFS) of Zinc(II)-Bound Pa DDAH. Samples for EXAFS [~1 mM, 20% (v/v) glycerol] were loaded into Lucite cuvettes with 6 μm polypropylene windows and frozen rapidly in liquid nitrogen. X-ray absorption spectra were measured at the National Synchrotron Light Source (NSLS), beamline X9B, with a Si(111) double-crystal monochromator; harmonic rejection was accomplished using a Ni focusing mirror. Fluorescence excitation spectra for all samples were measured with a 13-element solid-state Ge detector array. Samples were held at ~15 K in a Displex cryostat. EXAFS data collection and reduction were performed according to published procedures (*31*) using the software package Sixpack (*32*).

Nonlinear least-squares fits to Fourier-filtered EXAFS data are reported in Table 2; fits to unfiltered data gave similar results. Theoretical amplitude and phase functions, $A_s(k)$-$\exp(-2R_{as}/\lambda)$ and $\phi_{as}(k)$, were calculated using FEFF version 8.00 (*33*, *34*). The Zn−N (0.78) and Zn−S (0.91) scale factors and the threshold energy ($\Delta E_0 = -21$ eV) were held fixed at experimentally determined values. Fits were obtained for all reasonable coordination numbers, allowing for only the internuclear distance, R_{as}, and the Debye−Waller factor, σ_{as}^2, to vary for each shell of atoms. Multiple-scattering contributions from histidine ligands were approximated using published procedures (*31*). The four paths reported in Table 2 represent the sum of multiple-scattering contributions of 140 total paths. No physical label can be meaningfully applied to these combined paths.

UV−Vis Spectroscopy of Cobalt(II)-Bound Pa DDAH. Using a quartz microcuvette and a Cary 50 UV−vis spectrophotometer (Varian, Inc.), absorbance scans (300−800 nm) were recorded for wild-type (260 μM) and C249S mutant (190 μM) *Pa* DDAH in HEPES buffer (10 mM) and KCl (100 mM) at 25 °C and pH 7.3 upon the addition of $CoCl_2$ (40−860 μM). Baseline corrections were made using control solutions prepared without the protein component. To obtain difference spectra, the absorption values of the protein samples were subtracted, at each wavelength, from the resulting absorbance values after the addition of $CoCl_2$. To determine the apparent extinction coefficients for absorbance changes at 340 and 600 nm and to obtain the apparent dissociation constant for cobalt(II) binding, the absorbance changes at each of these two wavelengths, determined in three separate experiments, were fit to Beer's law (eq 11), where l is the path length of the cuvette (1 cm) and $[E\cdot Co^{2+}]$ is defined by eq 12 because the protein and ligand concentrations are of similar magnitude

$$Abs = \epsilon l[E\cdot Co^{2+}] \quad (11)$$

$$[E\cdot Co^{2+}] = [([E] + [CoCl_2] + K_d) - \sqrt{([E] + [CoCl_2] + K_d)^2 - 4[E][CoCl_2]}]/2 \quad (12)$$

RESULTS

pH Dependence of Pa DDAH-Catalyzed Substrate Hydrolysis. The k_{cat}/K_M values determined for *S*-methyl-L-thioctirulline and N^{ω}-methyl-L-arginine hydrolysis (Figure 1A) both showed a bell-shaped pH dependence that was fit to two apparent pK_a values. The fitted pK_a values for *S*-methyl-L-thiocitrulline were 7.4 ± 0.2 for the ascending limb (slope of 0.8) and 8.8 ± 0.2 for the descending limb, with a limiting nonzero plateau (0.2 s^{-1} mM^{-1}) at low pH. The fitted pK_a values for N^{ω}-methyl-L-arginine were 7.9 ± 0.3 for the ascending limb (slope of 1) and 9.3 ± 0.6 for the descending limb. Because these pairs of fitted pK_a values are closer than 3 units, Segel's method was used to calculate corrected pK_a values of 8.0 and 8.2 for *S*-methyl-L-thiocitrulline hydrolysis and 8.5 and 8.7 for N^{ω}-methyl-L-arginine hydrolysis.

The k_{cat} values determined for N^{ω}-methyl-L-arginine hydrolysis (Figure 1B) showed bell-shaped pH dependence and were fit to two apparent pK_a values: 6.1 ± 0.1 for the ascending limb (slope of 1) and 9.4 ± 0.1 for the descending limb. The k_{cat} values determined for *S*-methyl-L-thiocitrulline hydrolysis (Figure 1B) were best fit to one apparent pK_a of 5.6 ± 0.1 for the ascending limb (slope of 0.2) and a limiting nonzero plateau ($k_{min} = 0.6$ s^{-1}) at low pH values. *Pa* DDAH showed linear initial rates for substrate hydrolysis between pH values of 4.5−9.5, but at more acidic or alkaline pH

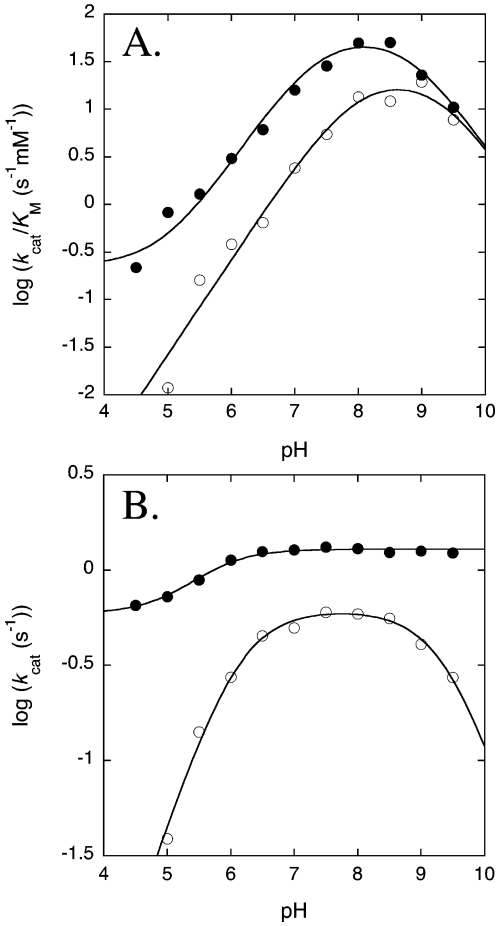

FIGURE 1: pH-rate profiles for substrate hydrolysis by wild-type *Pa* DDAH. (A) k_{cat}/K_M values for *S*-methyl-L-thiocitrulline (●) are fit to two corrected apparent pK_a values of 8.0 and 8.2, and the k_{cat}/K_M values for N^{ω}-methyl-L-arginine (○) are fit to two corrected pK_a values of 8.5 and 8.7 (see the Materials and Methods for details). (B) k_{cat} values for hydrolysis of *S*-methyl-L-thiocitrulline (●) are fit to one apparent pK_a of 5.6 for the ascending limb (slope of 0.2) and a nonzero plateau (0.6 s^{-1}) at low pH. The k_{cat} values for hydrolysis of N^{ω}-methyl-L-arginine (○) are fit to apparent pK_a values of 6.1 for the ascending limb (slope of 1) and 9.4 for the descending limb.

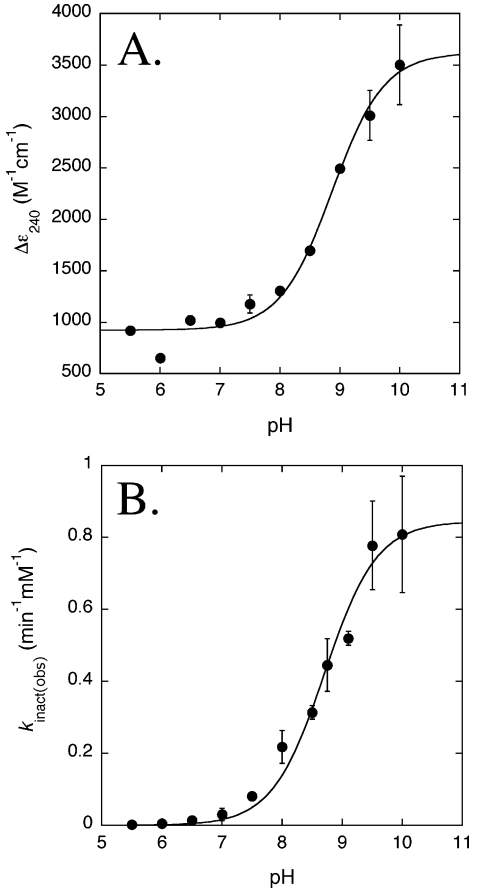

FIGURE 2: Determination of the pK_a of Cys249. (A) UV−vis difference spectroscopy at 240 nm between wild-type *Pa* DDAH and the C249S mutant, showing a pH-dependent increase in absorbance with an apparent pK_a of 8.9 because of thiolate formation. (B) Observed rates for inactivation of wild-type *Pa* DDAH by the thiol modification reagent iodoacetamide, showing a pH-dependent increase with an apparent pK_a of 8.7.

values, the enzyme was not active or displayed nonlinear kinetics, suggesting enzyme inactivation.

UV−Vis Difference Spectroscopy of Apoproteins. To follow the absorbance changes that occur at 240 nm because of pH-induced deprotonation at the thiol side chain of Cys249, differences in absorbance at 240 nm between wild-type and a C249S mutant *Pa* DDAH were determined (Figure 2A). A pH-dependent increase in absorbance at 240 nm was observed with an apparent pK_a of 8.9 ± 0.2 and $\Delta\epsilon_{240(max)}$ of 3600 ± 100 M^{-1} cm^{-1}. These experimentally determined values are consistent with typical pK_a values for unperturbed noncatalytic cysteine residues (*29*) and with ϵ_{240} values for 1 equiv of thiolate (*35*).

pH Dependence of Pa DDAH Inactivation by Iodoacetamide. Under our experimental conditions, plots of the pseudo-first-order inactivation rate constants with respect to the iodoacetamide concentration were linear, indicating second-order kinetics. Consequently, the second-order rate constants for inactivation at various pH values were determined. The addition of N^{ω}-methyl-L-arginine (2.5 mM) to an incubation mixture at pH 8.5 can prevent inactivation by iodoacetamide (Supporting Information), indicating that inactivation is due to modification at the active site. The rate of *Pa* DDAH inactivation by iodoacetamide increased at higher pH values (Figure 2B) and showed one apparent pK_a value of 8.7 ± 0.1, matching the apparent pK_a observed for the active-site Cys249 using UV−vis difference spectroscopy (Figure 2A). Fits of these data to a two pK_a model did not result in a statistically significant improvement (*F*-test). Using similar methods, attempts to obtain pseudo-first-order rate constants for inactivation by 2-chloroacetamidine, a known affinity label (*25*), were unsuccessful because of the rapid inactivation rates at high pH.

Mass Spectrometry of Quenched Reactions. Previous studies have shown that steady-state reactions of *Pa* DDAH with an activated substrate, *S*-methyl-L-thiocitrulline, can be acid-quenched to trap a transient covalent adduct of +157 Da that accumulates during turnover and may be a catalytic intermediate in the enzymatic mechanism (Scheme 1) (*20*). Here, incubation mixtures of both the wild-type and H162G proteins with the activated substrate *S*-methyl-L-thiocitrulline show the presence of the +157 Da adduct, within error (Table 1). However, incubation of these proteins with the naturally occurring substrate N^{ω},N^{ω}-dimethyl-L-arginine only resulted in accumulation of a +157 Da adduct with the wild-type protein. Incubations of this natural substrate with the H162G mutant only resulted in a mass matching that of the

Table 1: Summary of Major Ions Observed in ESI−MS Spectra of Acid-Quenched Steady-State Reactions with Wild-Type or H162G *Pa* DDAH and Various Substrates

substrate used in incubations	incubations with wild-type *Pa* DDAH[a] observed mass (Da)[b]	incubations with H162G *Pa* DDAH[a] observed mass (Da)[b]
control (without substrate)	30 495	30 415
N^{ω},N^{ω}-dimethyl-L-arginine	30 652	30 416
S-methyl-L-thiocitrulline	30 653	30 573

[a] The theoretical calculated mass for wild-type *Pa* DDAH is 30 403, and the theoretical calculated mass for H162G mutant *Pa* DDAH is 30 423. [b] The major ion peaks from deconvoluted ESI−MS spectra are reported with errors of ±10 Da. All reactions were completed at pH 8 prior to the acid quench.

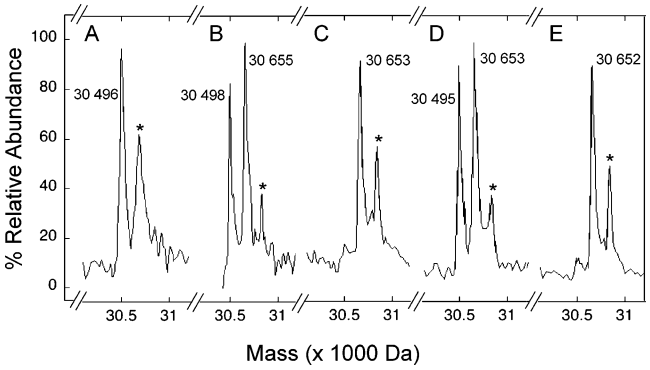

FIGURE 3: Deconvoluted ESI−MS spectra of trapped reactions with wild-type *Pa* DDAH. Steady-state reactions of wild-type *Pa* DDAH and N^{ω}-methyl-L-arginine at pH 5.5 (A) and pH 8.0 (B), N^{ω},N^{ω}-dimethyl-L-arginine at pH 8.0 (C), and *S*-methyl-L-thiocitrulline at pH 5.5 (D) and 8.0 (E) were acid-trapped and then analyzed by ESI−MS to detect any accumulation of a covalent adduct during turnover. Marked (*) peaks are attributable to a smaller fraction of nonenzymatically Nα-gluconoylated protein modified during expression. The calculated mass for unmodified wild-type *Pa* DDAH after removal of the N-terminal methionine is 30 503 Da. The expected mass of the proposed covalent intermediate is 30 660 Da. Representative ESI−MS plots are shown and typically have an error of ±10 Da.

unmodified enzyme, even when incubations were repeated at a pH value (9.5) higher than an unperturbed thiol pK_a.

This trapping technique was also used to identify the major species that accumulate during steady-state turnover by wild-type *Pa* DDAH at two different pH values (Figure 3).[2] At pH 5.5, trapping steady-state reactions of N^{ω}-methyl-L-arginine during turnover results only in protein that does not contain the +157 Da adduct (Figure 3A). However, when repeated at pH 8.0, trapping of these reactions results in a significant fraction of the enzyme in which the +157 Da covalent adduct accumulates (Figure 3B). At pH 5.5, trapping of reactions with *S*-methyl-L-thiocitrulline shows that a mixture of unmodified enzyme and covalent adduct is present (Figure 3D), but in reactions at a higher pH (8.0), almost all of the enzyme is trapped as the +157 Da covalent adduct (Figure 3E). At pH 8.0, trapping of reactions with N^{ω},N^{ω}-dimethyl-L-arginine (Figure 3C) also result in trapping almost all of the enzyme with the covalent adduct. Because the amount of covalent adduct that accumulates at high pH varies

[2] In each figure panel, there is an additional component (marked by an asterisk) that is due to nonenzymatic N-terminal gluconoylation of *Pa* DDAH, which occurs during protein expression but does not adversely affect catalysis. This modification has previously been described in detail and is not considered further here (*20*, *36*).

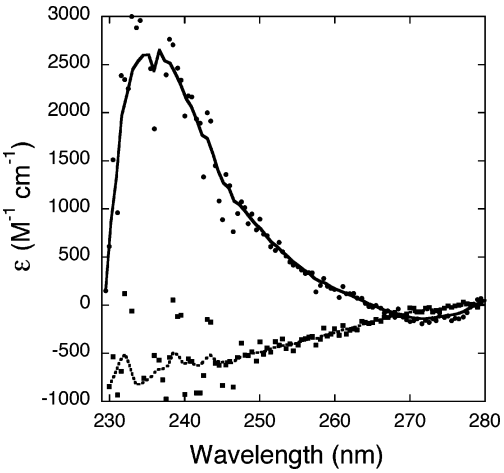

FIGURE 4: UV−vis difference spectra of *Pa* DDAH upon ligand binding. Spectra of L-citrulline-bound proteins are subtracted from L-lysine-bound proteins using both wild-type (●, —) and C249S mutant (■, - - -) *Pa* DDAH, indicating an increase of absorbance at 235 nm upon L-lysine binding to wild-type *Pa* DDAH at pH 7.3.

with the substrate, the k_{cat} and K_M values for N^{ω}-methyl-L-arginine (0.59 ± 0.01 s^{-1}, 44 ± 4 μM), N^{ω},N^{ω}-dimethyl-L-arginine (1.27 ± 0.04 s^{-1}, 39 ± 9 μM), and *S*-methyl-L-thiocitrulline (1.30 ± 0.04 s^{-1}, 26 ± 4 μM) were all determined at a single pH of 8.0 for comparison.

Inhibition of Pa DDAH by L-Lysine. L-Lysine was examined as a potential competitive inhibitor. A double-reciprocal plot of $(1/v_o)\times[E]$ versus 1/[S], determined at different L-lysine concentrations showed linear fits that intersect at the *y* axis, consistent with competitive inhibition (Supporting Information). Nonlinear fits to a competitive inhibition model determined a K_i for L-lysine inhibition of 4.0 ± 0.3 mM at pH 7.3. Previously, L-citrulline was determined to be a competitive inhibitor of *Pa* DDAH (*19*) with a K_i of 8.4 ± 0.5 mM at pH 7.3 (*24*).

UV−Vis Difference Spectroscopy of Ligand-Bound Proteins. Changes in absorbance near 240 nm, which are reflective of thiol deprotonation (*35*), were determined by subtracting spectra of L-citrulline-bound *Pa* DDAH from L-lysine-bound *Pa* DDAH. The ligand concentrations used were 2.5-fold higher than their K_i values as determined by competitive inhibition, resulting in ~70% saturation. These difference spectra showed a relative increase in absorbance with a λ_{max} near 235 nm and an apparent extinction coefficient of 3000 M^{-1} cm^{-1} (calcd 4300 M^{-1} cm^{-1} at full occupancy), consistent with deprotonation of 1 equiv of thiol upon L-lysine binding (Figure 4). Parallel experiments with the C249S mutant did not show a similar increase in absorbance, indicating that Cys249 is likely the thiol that becomes deprotonated upon ligand binding. The structure of C249S *Pa* DDAH has previously been reported and shows that this protein structure is comparable to the wild type and capable of binding L-citrulline at the active site (*19*).

Inhibition of Pa DDAH by Zinc(II). Initial rates were used to determine the IC_{50} value (8.8 ± 0.4 μM) for zinc acetate inhibition of *Pa* DDAH-catalyzed hydrolysis at subsaturating conditions of the substrate. Additional studies (below) show that the inhibitory metal-binding site is at the active site; therefore, assuming competitive inhibition and using the K_M determined for *S*-methyl-L-thiocitrulline, the K_i value for

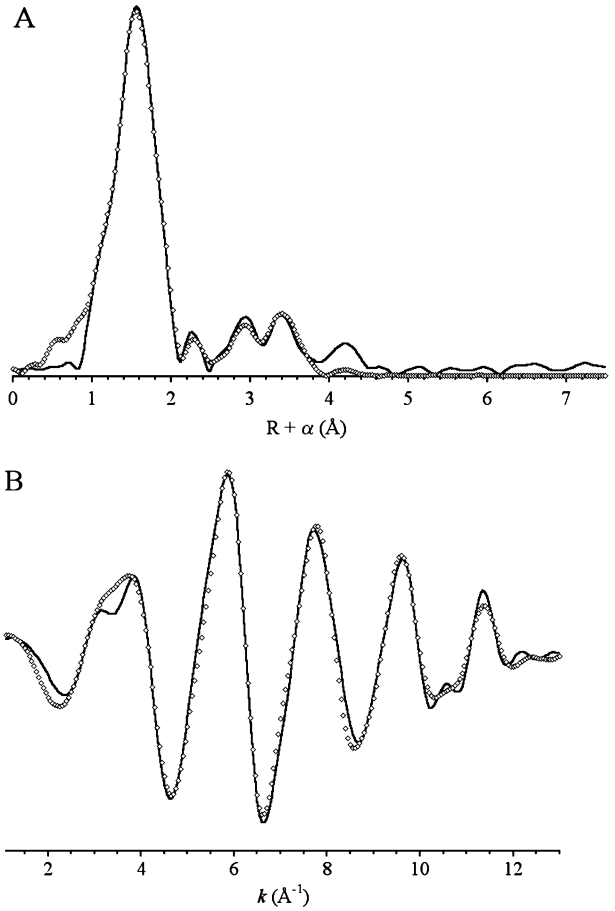

FIGURE 5: Fourier transforms (A) of experimental k^3-weighted EXAFS data (B) for Zn−DDAH (—) and best fit (◇).

zinc(II) was estimated to be 4.2 ± 0.2 μM (*30*). This value is quite similar to the K_i of 2.0 ± 0.8 μM initially reported for competitive inhibition of bovine DDAH-1 (*12*), although the zinc(II) dissociation constant for binding to bovine DDAH-1 was later determined to be 4.2 nM (*13*).

EXAFS of Zinc(II)-Bound Pa DDAH. Examination of the Zn K-edge EXAFS of Zn−DDAH shows a broad first shell peak (Figure 5A), indicative of heterogeneity in the coordination sphere of the metal. Also apparent are a series of features to higher *R* consistent with imidazole coordination. Fits to Fourier-filtered first shell data with only low-*Z* (N/O) scatterers indicate an average coordination number of 4 with an average bond length of 2.04 Å. This fit inadequately reproduced the breadth of the first shell peak in the FT. Inclusion of a single sulfur donor, while maintaining an overall coordination number of 4, resulted in a dramatic improvement in the visual quality of the fit and a 6-fold reduction in the fit residual (fits 1 and 2 in Table 2). Multiple-scattering fits including a mixed first shell of three N/O and one S donor and varying numbers of imidazole ligands indicate the presence of 1 ± 0.5 histidine ligands to the Zn ion. The fits shown in Figure 5 correspond to fit 3 in Table 2.

UV−Vis Spectroscopy of Cobalt(II)-Bound Pa DDAH. Spectral changes upon the addition of $CoCl_2$ to *Pa* DDAH show the formation of a new absorbance band at 340 nm and a broad absorption band at 500−650 nm (Figure 6A). The features at 340 and 600 nm both appear to saturate with matching apparent K_d values for cobalt(II) binding of 80 ± 10 and 80 ± 20 μM, respectively (Figure 6B). The apparent extinction coefficient at 340 nm is calculated to be 860 ± 30 M^{-1} cm^{-1}, similar in magnitude to the extinction coefficients reported for 1 equiv of thiolate binding to cobalt(II) (*37*−*39*). Additionally, the broad feature between 500 and 650 nm has a calculated extinction coefficient at 600 nm of 270 ± 10 M^{-1} cm^{-1}, which has a magnitude consistent with 4- or 5-coordinate cobalt(II) complexes (*37*, *38*, *40*, *41*). Parallel experiments with a C249S mutant do not show either of the spectral features at 340 or 600 nm (Figure 6C), indicating that cobalt(II) binding likely occurs at the active site. Precipitation is obvious at concentrations of $CoCl_2$ greater than 1 mM, precluding experiments at higher metal concentrations.

Table 2: EXAFS Curve-Fitting Results for Zn−DDAH[a]

fit	model	Zn−N/O	Zn−S	Zn−His[b]	R_f[c]	R_u
1	4 N/O	2.04 (3.6)			129	197
2	3 N/O + 1 S	2.01 (3.2)	2.23 (4.2)		21	87
3	3 N/O + 1 S (1 His)	2.01 (4.1)	2.23 (4.9)	2.92 (5.0), 3.19 (5.0) 4.11 (8.2), 4.41 (17)	38	49

[a] Distances (Å) and disorder parameters [in parentheses, σ^2 (10^{-3} Å^2)] derive from integer coordination number fits to filtered EXAFS data: Δk = 1−13 Å^{-1}, ΔR = 0.8−2.1 Å (fits 1−2) and ΔR = 0.1−4.5 Å (fit 3). [b] Multiple-scattering paths represent the combined paths described in the Materials and Methods. [c] Goodness of fit (R_f for fits to filtered data and R_u for fits to unfiltered data) defined as $1000\sum_{i=1}^{N}(\chi i_{calc}/\chi i_{obs})^2$, where *N* is the number of data points.

DISCUSSION

Enzymes in the amidinotransferase superfamily have been proposed to share similar catalytic mechanisms (*21*). In these mechanisms, an active-site cysteine residue (Cys249 in *Pa* DDAH) acts as a catalytic nucleophile that attacks the guanidino carbon of each substrate to form a covalent thiouronium intermediate. For example, a transient covalent adduct between Cys249 and a substrate of DDAH has been trapped and characterized, consistent with the proposal that this residue serves as a nucleophile (*20*). Covalent intermediates with active-site cysteine residues have also been characterized in other superfamily members (*15*−*18*). However, because the activity of these enzymes is generally measured at neutral or acidic pH values, it is not clear why the active-site cysteine residue is a good nucleophile or which residues are responsible for lowering its pK_a to facilitate deprotonation to the anionic thiolate. In most cysteine proteases, active-site cysteine and histidine residues make a pre-formed ion pair, resulting in a deprotonated thiolate with a pK_a of 3−4, which is activated in the resting enzyme and poised for attack on the substrate (*42*). A pre-formed ion-pair mechanism has been suggested as one possibility in *Pa* DDAH (*19*), but this mechanism is problematic. The crystal structure of *Pa* DDAH (*19*) indicates that there are no protein residues neighboring Cys249 that would be expected to lower the pK_a of this cysteine. In fact, the active-site His162 is more than 6 Å away from the side chain of a C249S mutation, and the product binds directly between these two residues. This long distance makes the proposal of a pre-formed Cys−His ion pair in *Pa* DDAH an unlikely prospect unless there are conformational changes in the ligand-free wild-type protein. The ionization state of Cys249 in the resting enzyme has not previously been reported, but

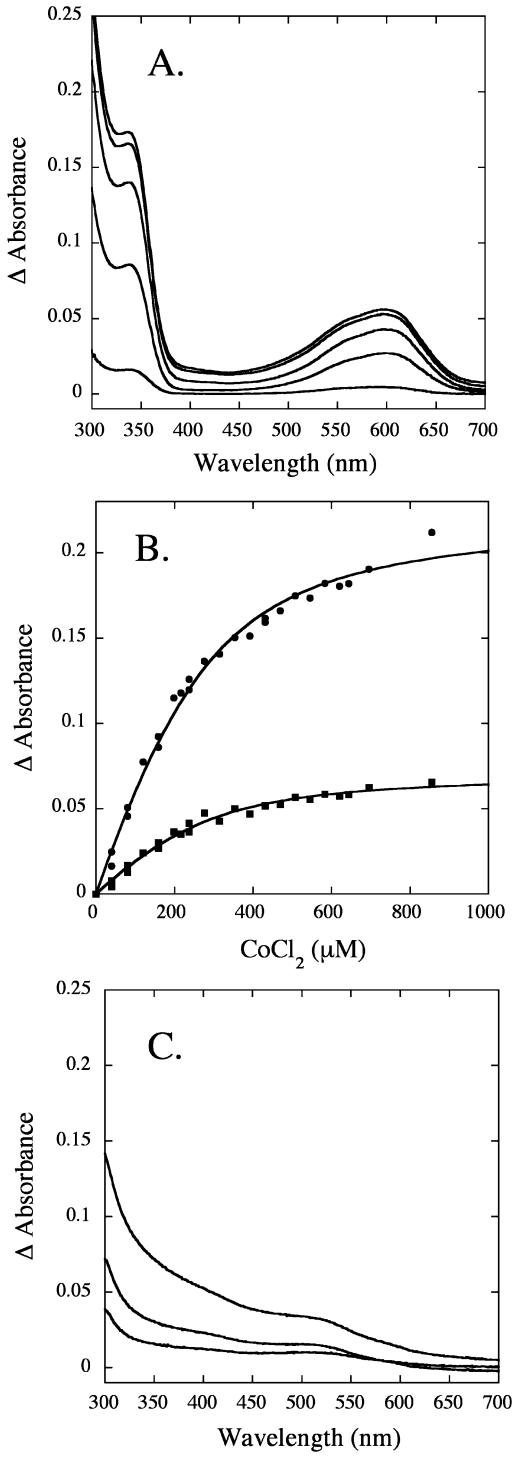

FIGURE 6: UV−vis spectra of cobalt(II) binding to *Pa* DDAH. (A) UV−vis difference spectra are determined by subtracting the spectrum of apo *Pa* DDAH from samples containing *Pa* DDAH (260 μM) and 40, 160, 320, 470, and 540 μM $CoCl_2$, resulting in increasing absorbance values. (B) Increases in absorbance at 340 nm (●) and 600 nm (■) upon the addition of $CoCl_2$ to *Pa* DDAH are fit as described in the Materials and Methods to yield apparent extinction coefficients of ϵ_{340} (860 ± 30 M^{-1} cm^{-1}) and ϵ_{600} (270 ± 10 M^{-1} cm^{-1}) and a K_d (80 ± 20 μM) for cobalt(II) binding. (C) UV−vis difference spectroscopy subtracting the spectrum of apo C249S *Pa* DDAH from samples containing C249S *Pa* DDAH (190 μM) and 220, 430, and 640 mM $CoCl_2$. Some precipitation is observed at higher $CoCl_2$ concentrations as evidenced by the increase in the baseline.

determining the pK_a of this residue is important for understanding the catalytic mechanism and designing specific inhibitors. Moreover, the nucleophilicity of this residue will influence its sensitivity to oxidation, nitrosation, and metal binding in proposed physiological regulatory mechanisms.

Our hypothesis is that *Pa* DDAH uses a substrate-assisted mechanism (*43*) in which Cys249 is protonated and neutral in the resting state but that binding of the positively charged guanidinium of the substrate adjacent to Cys249 depresses the pK_a of this residue and induces its deprotonation to the thiolate, thereby activating the catalytic nucleophile. The proton from Cys249 is lost either to the solvent or to an unidentified general base. To test this model, we investigated the protonation state of the active-site Cys249 in the resting enzyme and in the substrate- (and inhibitor-) bound enzyme and also tested the importance of the neighboring His162 residue.

The pH-dependent behavior of k_{cat}/K_M (Figure 1A) was used to follow ionizations in the ligand-free enzyme and the free substrate. An activated substrate, *S*-methyl-L-thiocitrulline, and a naturally occurring substrate, N^{ω}-methyl-L-arginine, both display narrow bell-shaped curves, with apparent pK_a values of 8 and 8.5 for the ascending limbs and 8.2 and 8.7 for the descending limbs, respectively. The *S*-methyl-L-thiocitrulline data is best fit with a nonzero plateau at low pH, suggesting that two ionization forms of *Pa* DDAH are active with this substrate. With both substrates, the apparent pK_a for the ascending limb is 8 or higher, consistent with Cys249 being predominantly neutral at pH 7. Without additional data, specifically assigning one of the apparent pK_a values to Cys249 ionization is somewhat problematic because of the possibility of reverse protonation states or a pH-dependent change in the rate-limiting step (*44*).

To circumvent these problems, we directly determined the pK_a of the active-site cysteine in the resting enzyme by using UV−vis difference spectroscopy between wild-type *Pa* DDAH and a C249S mutant. Thiolate anions absorb more strongly ($\epsilon_{240} \approx 4000$ M^{-1} cm^{-1}) than neutral protonated thiols ($\epsilon_{240} \approx 50$ M^{-1} cm^{-1}) (*35*), and UV−vis difference spectroscopy of wild-type and C249S mutant enzymes allow for the measurement of absorbance differences specifically because of changes in ionization at Cys249, eliminating interference from other protein residues. This technique has been used to determine the pK_a of specific cysteine residues in a variety of other enzymes (*27*, *45*, *46*). After measuring the difference spectra at different pH values where *Pa* DDAH remains stable, we observed a pH-dependent absorption difference at 240 nm with an apparent pK_a of 8.9, which can be assigned to the active-site cysteine (Figure 2A). We also determined a similar apparent pK_a value of 8.7 for inactivation of *Pa* DDAH by the neutral inactivator iodoacetamide (Figure 2B). All of our results indicate that the pK_a of the active-site cysteine is not significantly perturbed from that of typical noncatalytic cysteine residues. At pH 7, the neutral protonated form of the active-site cysteine predominates.

To determine the pH dependence of *Pa* DDAH catalysis when the substrate is bound at the active site, the pH-rate dependence for hydrolysis of two substrates, *S*-methyl-L-thiocitrulline and N^{ω}-methyl-L-arginine, was measured under k_{cat} conditions (Figure 1B). Both of these substrates show similar ascending limbs with apparent pK_a values of 5.6 and 6.1, respectively. However, only N^{ω}-methyl-L-arginine shows a descending limb at alkaline pH values. One possible

interpretation of these pH-rate profiles is that they reflect ionization of essential groups in the enzyme−substrate complex and that the apparent pK_a of the ascending limb is due to the ionization of Cys249, which would be expected to have a substantially shifted pK_a value when the positively charged guanidinium of the substrate is held in close proximity. If this interpretation is correct, then binding of the substrate would be responsible for lowering the Cys249 pK_a value by 2.8 units (from 8.9 to 6.1) reflecting a $\Delta\Delta G_{K_a}$ of 3.8 kcal/mol, similar to the typical range of $\Delta\Delta G$ values (3−5 kcal/mol) reported for buried salt bridges (*29*) and smaller than the 5−6 pH unit shift seen in the imidzaolium−thiolate ion pair of most cysteine proteases (*42*). It is likely that the active-site Glu65 and Asp66 residues could attenuate the full positive charge of bound ligands.

Alternatively, instead of reflecting the ionization of particular groups, steady-state pH-rate curves can also reflect kinetic pK_a values, which are instead due to changes in the rate-limiting step of the overall reaction (*29*). This seems likely for *S*-methyl-L-thiocitrulline, which has a slope considerably less than 1. A change in the rate-limiting step may also occur with N^{ω}-methyl-L-arginine. Acid-quenched steady-state reactions with N^{ω}-methyl-L-arginine show that at low pH values (5.5) only the unmodified enzyme is present (Figure 3A) but, at higher pH values (8.0), a significant amount of covalent adduct is detected (Figure 3B). Accumulation of the covalent adduct at higher pH values suggests that intermediate decay becomes at least partially rate-determining under these experimental conditions. Nonetheless, these results are still consistent with the activation of the catalytic nucleophile in the saturated enzyme at pH values lower than the pK_a determined for Cys249 in the resting enzyme. It should be noted that, at the pH optimum of *Pa* DDAH, we are able to trap a covalent adduct that accumulates during steady-state turnover of N^{ω}-methyl- and asymmetrical N^{ω},N^{ω}-dimethyl-L-arginine (parts B and C of Figure 3), indicating that the proposed covalent intermediate can be trapped using naturally occurring substrates and not only with an activated artificial substrate (*20*). Reactions with *S*-methyl-L-thiocitrulline show a similar pH-dependent increase in the amount of trapped intermediate, but the presence of some intermediates at low pH and the nonzero plateau of the k_{cat} pH curve may indicate that the neutral thiol retains a lower level of activity toward this activated substrate. The varying peak ratios of the unmodified to the intermediate-trapped enzyme in these steady-state trapping experiments are likely due to differences in the rates of intermediate formation and will be explored in future transient kinetic studies.

A direct approach was used to confirm that binding of cationic ligands can induce deprotonation of Cys249. Difference UV−vis spectroscopy of *Pa* DDAH with a positively charged ligand bound and with a neutral ligand bound is used to reveal differences in the protonation state of cysteine. Toward these ends, we demonstrate that L-lysine, which has a positively charged side chain at pH 7.3, can serve as a competitive inhibitor of *Pa* DDAH. A competitive inhibitor with a neutral side chain, L-citrulline, has already been reported for *Pa* DDAH (*19*, *24*). This pair of ligands was used for UV−vis difference spectroscopy and shows that binding a cationic ligand to wild-type *Pa* DDAH results in an increase of absorbance near 240 nm relative to the binding of a neutral ligand, and the magnitude of this increase is consistent with the deprotonation of one cysteine side chain (Figure 4). Difference spectroscopy of these two ligands with a C249S mutant showed no such change, indicating that this thiolate is formed at the active site. These results directly show that binding a positively charged ligand stabilizes the anionic form of Cys249 and are consistent with a substrate-assisted mechanism, where binding of a cationic ligand lowers the pK_a of the active-site cysteine, favoring deprotonation and activation of this residue as a catalytic anionic nucleophile. It has not yet been determined whether a general base assists in deprotonation of this thiol or if the proton is lost directly to the solvent.

We also investigated whether binding cationic metal ions could stabilize the anionic Cys249 thiolate. Various divalent metals have been reported as inhibitors of mammalian DDAH isoforms (*13*, *14*) and also of human peptidylarginine deiminase (*22*). Here, we report that zinc(II) can inhibit *Pa* DDAH with an estimated K_i of 4 μM. Bovine DDAH-1 appears to be much more sensitive to zinc inhibition with a dissociation constant of 4.2 nM (*13*). Knipp et al. propose that, upon significant conformational rearrangement, a zinc-binding site in bovine DDAH-1 is formed, which consists of the active-site cysteine (bovine Cys273) that corresponds to *Pa* DDAH Cys249, a distant cysteine (bovine Cys221) that is also conserved in *Pa* DDAH (Cys205), and two N/O ligands, with no evidence for a coordinating histidine (*9*, *13*). Because of the large difference in zinc affinity observed between bovine and bacterial DDAH isoforms, we used EXAFS to determine whether the inhibitory metal ion is bound at the active-site Cys249 of *Pa* DDAH or at a distant site.

The EXAFS data clearly indicate the presence of one cysteine thiolate and one histidine imidazole in the coordination sphere of the inhibitory zinc ion. The overall average bond length is most consistent with four coordination of the zinc ion, with the two remaining ligands most likely being water molecules or neighboring carboxylates, although no clear Zn−C interaction could be identified in the EXAFS. The unusually short Zn−S bond length is consistent with direct coordination to the active-site cysteine, reflecting the nucleophilicity of the DDAH active-site sulfur.

Building on the experimental finding that the zinc-binding site of *Pa* DDAH contains one cysteine residue, one histidine residue, and two (N/O) ligands, the structure of *Pa* DDAH (*19*) was used to find pairs of cysteine and histidine residues that occur close in space without requiring significant conformational rearrangement. Using this criteria, only two pairs of cysteine and histidine residues were identified as likely zinc-binding sites: the active-site Cys249/His162 pair and a Cys74/His148 pair that is found more than 20 Å from the active site and is also distant from the dimerization interface (*47*). To determine which of these two possible sites may be responsible for inhibitory metal binding, we used cobalt(II) as a spectroscopic probe. Thiolate−cobalt(II) interactions result in the appearance of a ligand-to-metal charge transfer (LMCT) band near 340 nm (*37*−*39*). Hence, UV−vis spectroscopy was used to follow absorbance changes because of the binding of cobalt(II) to *Pa* DDAH. Using this method, an increase in absorbance at 340 nm was observed with a magnitude consistent with cobalt(II) binding to one thiolate (Figure 6). Also, the weak features observed

between 500 and 650 nm upon cobalt(II) binding to *Pa* DDAH are indicative of Laporte-forbidden cobalt(II) d−d transitions and have an extinction coefficient of 270 M^{-1} cm^{-1}, consistent with a 4- or 5-coordinate cobalt(II) site (*37*, *38*, *40*, *41*). The apparent dissociation constant for cobalt(II) appears to be higher than that measured for zinc(II); however, cobalt is often used as a spectroscopic probe for zinc-binding sites, and differences in affinity between these two metals are not unusual. Notably, when difference spectroscopy of a C249S mutant is measured (Figure 6), no LMCT band is observed upon the addition of cobalt(II), indicating that the active-site Cys249/His162 pair is the major metal-binding site in *Pa* DDAH. Therefore, binding of metal ions to the bacterial *Pa* DDAH leads to inhibition of substrate turnover by competing for binding near the active-site residues, Cys249 and His162, and not to a more distant site as postulated in the mammalian bovine DDAH isoform (*9*). Importantly, binding of this cationic metal ion can also stabilize the active-site cysteine thiolate as evidenced by the appearance of the LMCT band, which requires a thiolate anion (*37*, *38*, *40*). In summary, binding cationic ligands at the active site can stabilize the formation of the anionic Cys249 thiolate.

The pH-rate behavior can also provide additional insight into the DDAH catalytic mechanism. The k_{cat} pH profiles for the two substrates tested here are markedly different at alkaline pH values. The k_{cat} values of N^{ω}-methyl-L-arginine show a descending limb with an apparent pK_a of 9.4, but those of *S*-methyl-L-thiocitrulline do not have a corresponding descending limb (Figure 1B). The major difference between these two substrates is their respective leaving groups, methylamine and methanethiol. While the methylamine leaving group likely requires protonation prior to or concomitant with C−N bond cleavage, protonation of the methanethiol leaving group may not be essential. This difference in leaving groups is likely reflected in their different response to changes in pH, with hydrolysis of N^{ω}-methyl-L-arginine slowing under alkaline conditions because of a lack of protonation of the leaving group. A similar technique of installing a thiol leaving group to overcome the need for general-acid catalysis was recently used in the study of hepatitis delta virus ribozyme (*48*). The residue responsible for protonating the leaving group during *Pa* DDAH catalysis has been proposed as His162 based on the crystal structure of the enzyme (*19*). This residue is well-placed to serve as a general acid during turnover. After the His162 residue protonates the leaving group, it may also play a second role as a general base to deprotonate a crystallographically observed water molecule, generating hydroxide for hydrolysis of the covalent thiouronium intermediate. This proposal is consistent with structural overlays of *Pa* DDAH and *Mycoplasma arginini* arginine deiminase (*16*). When overlayed, a crystallographic water molecule in *Pa* DDAH nearly superimposes with one of the terminal heteroatoms of the trapped tetrahedral intermediate in arginine deiminase, indicating that the observed water is indeed well-placed for attack on the covalent intermediate.

These two proposed roles for His162 in *Pa* DDAH catalysis can be tested experimentally. A mutant protein lacking this active-site histidine should be incapable of substrate turnover [as was previously reported for a H162N mutant (*19*)] but should be able to accumulate a stable intermediate under certain conditions. If protonation of the leaving group is not required for bond cleavage (as is expected for *S*-methyl-L-thiocitrulline), then a mutant protein lacking His162 should accumulate a stable thiouronium adduct because the mutant would not be able to generate a hydroxide for intermediate hydrolysis. However, if protonation of the leaving group is required (as is expected for N^{ω},N^{ω}-dimethyl-L-arginine), then no covalent adduct should accumulate because the leaving group would not be sufficiently stabilized by the mutant protein and the overall reaction would be blocked at an earlier step. This proposal was tested by incubating a H162G *Pa* DDAH mutant with *S*-methyl-L-thiocitrulline, which resulted in the accumulation of a stable covalent adduct that does not decay (Table 1). Incubation of the H162G mutant with the cationic inactivator 2-chloroacetamidine results in facile labeling of Cys249 (*25*), suggesting that His162 is not essential for maintaining the nucleophilicity of Cys249 as would be the case in a preformed ion-pair mechanism. In contrast to the results using *S*-methyl-L-thiocitrulline, incubation of the H162G mutant with N^{ω},N^{ω}-dimethyl-L-arginine does not result in the accumulation of a covalent adduct (Table 1). These results are consistent with a dual role for His162 in the catalytic mechanism of *Pa* DDAH: this residue could act as a general acid to protonate the leaving group of the substrate and subsequently as a general base to deprotonate a water molecule for hydrolysis of the covalent thiouronium intermediate.

Just as cationic ligand binding can stabilize deprotonated Cys249, the positive charge of the thiouronium intermediate may also lower the pK_a of the hydrolytic water molecule in the second half of the reaction to assist deprotonation by His162. The pK_a values (*49*) of methylguanidine (13.4) and *S*-methylthiourea (9.8) can be used to estimate the change in pK_a from the guanidine group of the substrate to the pK_a of the covalent thiouronium intermediate. This comparison predicts a decrease of 3.6 units from that of the free substrate upon intermediate formation, resulting in a thiouronium adduct that is still positively charged at physiological pH values. The presence of active-site carboxylates including Glu65 and Asp66 may also attenuate this charge. Experimental work with another superfamily member, arginine deiminase, suggests that retaining a positive charge in the covalent intermediate may be important for intermediate hydrolysis. Arginine deiminase can hydrolyze L-canavanine as a slow substrate with a particularly stabilized covalent intermediate that is only very slowly hydrolyzed to release product (*50*). The pK_a of L-canavanine (7.01) is significantly lower than that of arginine (*49*). If the pK_a drops an additional 3.6 units upon intermediate formation, then the resulting covalent intermediate would be neutral at physiological pH values, would be much less electrophilic, and would not be able to favorably perturb the pK_a of the adjacent hydrolytic water molecule to facilitate hydrolysis, consistent with the long lifetime (*50*) of this intermediate. These experimental results argue that the positive charge of both the substrate and the intermediate plays an important part in the mechanism of these proteins.

Additionally, the substrate-assisted mechanism of *Pa* DDAH may partially explain why this enzyme only catalyzes hydrolysis of substituted guanidines to ureas and does not catalyze the subsequent hydrolysis of substituted ureas to

Scheme 2: Proposed Substrate-Assisted Mechanism of *Pa* DDAH

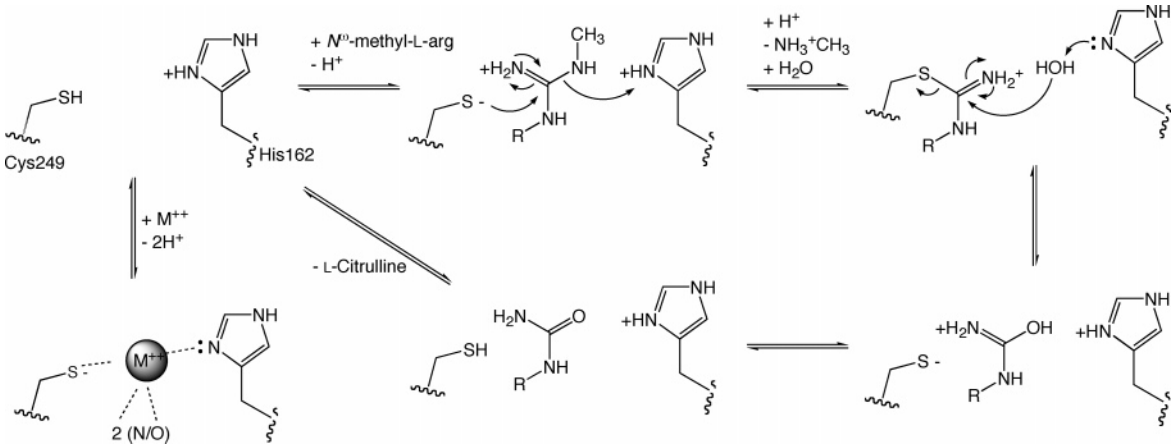

amines, a reaction that is catalyzed by *N*-succinylarginine dihydrolase (*51*), another amidinotransferase superfamily member. In the case of *Pa* DDAH, after formation of the neutral product citrulline, there would be no cationic charge left adjacent to the Cys249 to facilitate the activation of this nucleophile. Presumably, dihydrolases have alternative mechanisms for catalyzing hydrolysis of neutral substrates. As discussed elsewhere, the ionization properties of active-site residues in this superfamily of proteins appear to be very interdependent (*52*), and further studies will be required to understand exactly how the interplay of these residues promotes catalysis.

The results presented here support a substrate-assisted catalytic mechanism for *Pa* DDAH (Scheme 2) in which the active-site cysteine remains neutral until binding of a cationic substrate depresses the Cys249 pK_a sufficiently to trigger deprotonation and activation of this thiolate nucleophile. The proton from Cys249 is lost either to the solvent or to an unidentified general base. The active-site His162 appears to play a dual role in the mechanism: first, as a general acid to protonate the leaving group and, subsequently, as a general base to generate a hydroxide for hydrolysis of the covalent intermediate. In addition to providing a binding site for the substrate, these two residues also form a binding site for inhibitory metal ions that can stabilize the active-site thiolate. Many of the active-site residues are strongly conserved throughout the amidinotransferase superfamily, but it is not yet known whether other superfamily members also use substrate-assisted mechanisms. Despite conserved active-site residues, the pH-rate behavior of these superfamily members can be quite different. For example, arginine deiminase from *P. aeruginosa* shows optimum catalysis at pH values less than 6 (*52*); arginine deiminase from *Mycoplasma arthritidis* can function at pH values above 7 (*53*); and human peptidylarginine deiminase-4 has a narrow pH optimum at 7.6 (*22*). Even other DDAH isoforms such as those from a cow (*13*) and rat (*54*) appear to have different pH behavior than the bacterial DDAH studied here. Therefore, the generality of this mechanism is yet to be determined.

Ligand-induced cysteine deprotonation should be considered in the design of covalent inhibitors that target the active-site cysteine of related enzymes. For example, *Pa* DDAH inactivation rates are significantly higher for 2-chloroacetamidine at neutral pH than for iodoacetamide, despite the presence of a worse leaving group (data not shown). The related fluoroacetamidine affinity labels are much better inhibitors of peptidylarginine deiminase than their neutral analogues (*55*), and the possible role of electrostatics in the inhibition of arginine deiminase by canavanine has been proposed here and elsewhere (*50*). In addition to its importance to inhibitor design, the substrate-assisted mechanism of *Pa* DDAH may have physiological significance. S-Nitrosylation has been suggested as a physiological regulation mechanism of mammalian DDAH isoforms (*8*, *9*). However, neutral thiols are much less reactive to oxidation and nitrosation than anionic thiolates, suggesting that the neutral cysteine residue found in the resting state of this bacterial DDAH may be more resistant to inhibition by cellular oxidants than would be the case if this enzyme used a pre-formed ion pair in its mechanism. DDAH isoforms also appear to have significant differences in the coordination and affinity of inhibitory metal ions, and these differences could have physiological relevance. Further studies will be required to understand the origin and ramifications of the functional differences between amidinotransferase superfamily members.

It should be noted that the use of ligand-assisted cysteine deprotonation has also been proposed in unrelated enzymes. For example, recent studies of ubiquitin-conjugating enzymes suggest that a catalytic cysteine nucleophile is not deprotonated until the substrate is bound, and this mechanism was suggested to protect against nonspecific mistargeting of cellular proteins for degradation (*56*). The work presented here provides a clear example of one enzyme in the amidinotransferase superfamily, *Pa* DDAH, that uses a substrate-assisted mechanism to modulate the reactivity of an active-site cysteine nucleophile.

SUPPORTING INFORMATION AVAILABLE

Figure S1, showing competitive inhibition of *Pa* DDAH by L-lysine, and Figure S2 and experimental details, showing substrate protection against inactivation of *Pa* DDAH by iodoacetamide. This material is available free of charge via the Internet at http://pubs.acs.org.

REFERENCES

1. Cooke, J. P. (2004) Asymmetrical dimethylarginine: The Über marker? *Circulation 109*, 1813−1818.
2. Dayoub, H., Achan, V., Adimoolam, S., Jacobi, J., Stuehlinger, M. C., Wang, B. Y., Tsao, P. S., Kimoto, M., Vallance, P.,

Patterson, A. J., and Cooke, J. P. (2003) Dimethylarginine dimethylaminohydrolase regulates nitric oxide synthesis: Genetic and physiological evidence, *Circulation 108*, 3042−3047.
3. Cardounel, A. J., and Zweier, J. L. (2002) Endogenous methylarginines regulate neuronal nitric-oxide synthase and prevent excitotoxic injury, *J. Biol. Chem. 277*, 33995−34002.
4. Achan, V., Ho, H. K., Heeschen, C., Stuehlinger, M., Jang, J. J., Kimoto, M., Vallance, P., and Cooke, J. P. (2005) ADMA regulates angiogenesis: Genetic and metabolic evidence, *Vasc. Med. 10*, 7−14.
5. Kostourou, V., Robinson, S. P., Whitley, G. S., and Griffiths, J. R. (2003) Effects of overexpression of dimethylarginine dimethylaminohydrolase on tumor angiogenesis assessed by susceptibility magnetic resonance imaging, *Cancer Res. 63*, 4960−4966.
6. Kostourou, V., Robinson, S. P., Cartwright, J. E., and Whitley, G. S. (2002) Dimethylarginine dimethylaminohydrolase I enhances tumour growth and angiogenesis, *Br. J. Cancer 87*, 673−680.
7. Vallance, P., and Leiper, J. (2002) Blocking NO synthesis: How, where and why? *Nat. Rev. Drug Discovery 1*, 939−950.
8. Leiper, J., Murray-Rust, J., McDonald, N., and Vallance, P. (2002) S-Nitrosylation of dimethylarginine dimethylaminohydrolase regulates enzyme activity: Further interactions between nitric oxide synthase and dimethylarginine dimethylaminohydrolase, *Proc. Natl. Acad. Sci. U.S.A. 99*, 13527−13532.
9. Knipp, M., Braun, O., Gehrig, P. M., Sack, R., and Vasak, M. (2003) Zn(II)-free dimethylargininase-1 (DDAH-1) is inhibited upon specific Cys-S-nitrosylation, *J. Biol. Chem. 278*, 3410−3416.
10. Stuhlinger, M. C., Tsao, P. S., Her, J. H., Kimoto, M., Balint, R. F., and Cooke, J. P. (2001) Homocysteine impairs the nitric oxide synthase pathway: Role of asymmetric dimethylarginine, *Circulation 104*, 2569−2575.
11. Knipp, M., Braun, O., and Vasak, M. (2005) Searching for DDAH inhibitors: *S*-Nitroso-L-homocysteine is a chemical lead, *J. Am. Chem. Soc. 127*, 2372−2373.
12. Bogumil, R., Knipp, M., Fundel, S. M., and Vasak, M. (1998) Characterization of dimethylargininase from bovine brain: Evidence for a zinc binding site, *Biochemistry 37*, 4791−4798.
13. Knipp, M., Charnock, J. M., Garner, C. D., and Vasak, M. (2001) Structural and functional characterization of the Zn(II) site in dimethylargininase-1 (DDAH-1) from bovine brain. Zn(II) release activates DDAH-1, *J. Biol. Chem. 276*, 40449−40456.
14. Ogawa, T., Kimoto, M., and Sasaoka, K. (1989) Purification and properties of a new enzyme, N^G,N^G-dimethylarginine dimethylaminohydrolase, from rat kidney, *J. Biol. Chem. 264*, 10205−10209.
15. Lu, X., Galkin, A., Herzberg, O., and Dunaway-Mariano, D. (2004) Arginine deiminase uses an active-site cysteine in nucleophilic catalysis of L-arginine hydrolysis, *J. Am. Chem. Soc. 126*, 5374−5375.
16. Das, K., Butler, G. H., Kwiatkowski, V., Clark, A. D., Jr., Yadav, P., and Arnold, E. (2004) Crystal structures of arginine deiminase with covalent reaction intermediates; implications for catalytic mechanism, *Structure 12*, 657−667.
17. Smith, D. W., and Fahrney, D. E. (1978) Catalysis by arginine deiminase: Evidence for a covalent intermediate, *Biochem. Biophys. Res. Commun. 83*, 101−106.
18. Humm, A., Fritsche, E., Mann, K., Gohl, M., and Huber, R. (1997) Recombinant expression and isolation of human L-arginine:glycine amidinotransferase and identification of its active-site cysteine residue, *Biochem. J. 322* (part 3), 771−776.
19. Murray-Rust, J., Leiper, J., McAlister, M., Phelan, J., Tilley, S., Santa Maria, J., Vallance, P., and McDonald, N. (2001) Structural insights into the hydrolysis of cellular nitric oxide synthase inhibitors by dimethylarginine dimethylaminohydrolase, *Nat. Struct. Biol. 8*, 679−683.
20. Stone, E. M., Person, M. D., Costello, N. J., and Fast, W. (2005) Characterization of a transient covalent adduct formed during dimethylarginine dimethylaminohydrolase catalysis, *Biochemistry 44*, 7069−7078.
21. Shirai, H., Blundell, T. L., and Mizuguchi, K. (2001) A novel superfamily of enzymes that catalyze the modification of guanidino groups, *Trends Biochem. Sci. 26*, 465−468.
22. Kearney, P. L., Bhatia, M., Jones, N. G., Yuan, L., Glascock, M. C., Catchings, K. L., Yamada, M., and Thompson, P. R. (2005) Kinetic characterization of protein arginine deiminase 4: A transcriptional corepressor implicated in the onset and progression of rheumatoid arthritis. *Biochemistry 44*, 10570−10582.
23. Knipp, M., and Vasak, M. (2000) A colorimetric 96-well microtiter plate assay for the determination of enzymatically formed citrulline, *Anal. Biochem. 286*, 257−264.
24. Stone, E. M., and Fast, W. (2005) A continuous spectrophotometric assay for dimethylarginine dimethylaminohydrolase, *Anal. Biochem. 343*, 335−337.
25. Stone, E. M., Schaller, T. H., Bianchi, H., Person, M. D., and Fast, W. (2005) Inactivation of two diverse enzymes in the amidinotransferase superfamily by 2-chloroacetamidine: Dimethylargininase and peptidylarginine deiminase, *Biochemistry 44*, 13744−13752.
26. Segel, I. H. (1975) *Enzyme Kinetics*, John Wiley and Sons, Inc., New York.
27. Wang, P. F., McLeish, M. J., Kneen, M. M., Lee, G., and Kenyon, G. L. (2001) An unusually low pK_a for Cys282 in the active site of human muscle creatine kinase, *Biochemistry 40*, 11698−11705.
28. Malinen, A. M., Belogurov, G. A., Salminen, M., Baykov, A. A., and Lahti, R. (2004) Elucidating the role of conserved glutamates in H^+-pyrophosphatase of *Rhodospirillum rubrum*, *J. Biol. Chem. 279*, 26811−26816.
29. Fersht, A. (1999) *Structure and Mechanism in Protein Science*, W. H. Freeman and Company, New York.
30. Cheng, Y., and Prusoff, W. H. (1973) Relationship between the inhibition constant (K_I) and the concentration of inhibitor which causes 50% inhibition (I_{50}) of an enzymatic reaction, *Biochem. Pharmacol. 22*, 3099−3108.
31. Thomas, P. W., Stone, E. M., Costello, A. L., Tierney, D. L., and Fast, W. (2005) The quorum-quenching lactonase from *Bacillus thuringiensis* is a metalloprotein, *Biochemistry 44*, 7559−7569.
32. Sixpack is available free of charge from http://www-sssrl.slac.stanford.edu/~swebb/index.htm.
33. IFEFFIT is open-source software available from http://cars9.uchicago.edu/ifeffit.
34. Ankudinov, A. L., Ravel, B., Rehr, J. J., and Conradson, S. D. (1998) Real space multiple scattering calculation and interpretation of XANES, *Phys. Rev. B: Condens. Matter Mater. Phys. 58*, 7565−7576.
35. Polgar, L. (1974) Spectrophotometric determination of mercaptide ion, an activated form of SH-group in thiol enzymes, *FEBS Lett. 38*, 187−190.
36. Geoghegan, K. F., Dixon, H. B., Rosner, P. J., Hoth, L. R., Lanzetti, A. J., Borzilleri, K. A., Marr, E. S., Pezzullo, L. H., Martin, L. B., LeMotte, P. K., McColl, A. S., Kamath, A. V., and Stroh, J. G. (1999) Spontaneous α-*N*-6-phosphogluconoylation of a "His tag" in *Escherichia coli*: The cause of extra mass of 258 or 178 Da in fusion proteins, *Anal. Biochem. 267*, 169−184.
37. Maret, W., and Vallee, B. L. (1993) Cobalt as probe and label of proteins, *Methods Enzymol. 226*, 52−71.
38. Lever, A. B. P. (1984) *Inorganic Electronic Spectroscopy*, 2nd ed., Elsevier, Amsterdam, The Netherlands.
39. Alexander, R. S., Kiefer, L. L., Fierke, C. A., and Christianson, D. W. (1993) Engineering the zinc binding site of human carbonic anhydrase II: Structure of the His-94 → Cys apoenzyme in a new crystalline form, *Biochemistry 32*, 1510−1518.
40. Vallee, B. L., and Galdes, A. (1984) The metallobiochemistry of zinc enzymes, *Adv. Enzymol. Relat. Areas Mol. Biol. 56*, 283−430.
41. Garmer, D. R., and Krauss, M. (1993) *Ab initio* quantum chemical study of the cobalt d−d spectroscopy of several substituted zinc enzymes, *J. Am. Chem. Soc. 115*, 10247−10257.
42. Brocklehurst, K., Watts, A. B., Patel, M., and Thomas, E. W. (1998) Cysteine proteinases, in *Comprehensive Biological Catalysis* (Sinnott, M., Ed.) pp 381, Academic Press, New York.
43. Dall'Acqua, W., and Carter, P. (2000) Substrate-assisted catalysis: Molecular basis and biological significance, *Protein Sci. 9*, 1−9.
44. Cleland, W. W. (1977) Determining the chemical mechanisms of enzyme-catalyzed reactions by kinetic studies, *Adv. Enzymol. Relat. Areas Mol. Biol. 45*, 273−387.
45. Sarkany, Z., Szeltner, Z., and Polgar, L. (2001) Thiolate−imidazolium ion pair is not an obligatory catalytic entity of cysteine peptidases: The active site of picornain 3C, *Biochemistry 40*, 10601−10606.
46. Nelson, J. W., and Creighton, T. E. (1994) Reactivity and ionization of the active site cysteine residues of DsbA, a protein required for disulfide bond formation in vivo, *Biochemistry 33*, 5974−5983.
47. Plevin, M. J., Magalhaes, B. S., Harris, R., Sankar, A., Perkins, S. J., and Driscoll, P. C. (2004) Characterization and manipulation

of the *Pseudomonas aeruginosa* dimethylarginine dimethylaminohydrolase monomer−dimer equilibrium, *J. Mol. Biol. 341*, 171−184.
48. Das, S. R., and Piccirilli, J. A. (2005) General acid catalysis by the hepatitis delta virus ribozyme, *Nat. Chem. Biol. 1*, 45−52.
49. Jencks, W. P., and Regenstein, J. (1968) Ionization constants of acids and bases, in *Handbook of Biochemistry* (Sober, H. A., Ed.) pp J-148−J-189, CRC, Cleveland, OH.
50. Lu, X., Li, L., Feng, X., Wu, Y., Dunaway-Mariano, D., Engen, J. R., and Mariano, P. S. (2005) L-Canavanine is a time-controlled mechanism-based inhibitor of *Pseudomonas aeruginosa* arginine deiminase, *J. Am. Chem. Soc. 127*, 16412−16413.
51. Tocilj, A., Schrag, J. D., Li, Y., Schneider, B. L., Reitzer, L., Matte, A., and Cygler, M. (2005) Crystal structure of *N*-succinylarginine dihydrolase AstB, bound to substrate and product, an enzyme from the arginine catabolic pathway of *Escherichia coli*, *J. Biol. Chem. 280*, 15800−15808.
52. Galkin, A., Lu, X., Dunaway-Mariano, D., and Herzberg, O. (2005) Crystal structures representing the Michaelis complex and the thiouronium reaction intermediate of *Pseudomonas aeruginosa* arginine deiminase, *J. Biol. Chem. 280*, 34080−34087.
53. Weickmann, J. L., Himmel, M. E., Smith, D. W., and Fahrney, D. E. (1978) Arginine deiminase: Demonstration of two active sites and possible half-of-the-sites reactivity, *Biochem. Biophys. Res. Commun. 83*, 107−113.
54. Ogawa, T., Kimoto, M., Watanabe, H., and Sasaoka, K. (1987) Metabolism of N^G,N^G- and N^G,N'^G-dimethylarginine in rats, *Arch. Biochem. Biophys. 252*, 526−537.
55. Luo, Y., Knuckley, B., Lee, Y. H., Stallcup, M. R., and Thompson, P. R. (2006) A fluoroacetamidine-based inactivator of protein arginine deiminase 4: Design, synthesis, and in vitro and in vivo evaluation, *J. Am. Chem. Soc. 128*, 1092−1093.
56. Tolbert, B. S., Tajc, S. G., Webb, H., Snyder, J., Nielsen, J. E., Miller, B. L., and Basavappa, R. (2005) The active site cysteine of ubiquitin-conjugating enzymes has a significantly elevated pK_a: Functional implications, *Biochemistry 44*, 16385−16391.

BI052595M